Fabrication of Suspended Microchannel Resonators With Two-Photon Based 3D Printer

Professors: Guillermo Villanueva
Supervisor: Damien Maillard
Author: Leonardo Cele'

6 June, 2022

Contents

List of Figures

List of Tables

1 Introduction

1.1 Project objectives

The objective of this project is to optimize the fabrication of suspended microchannels with thin walls and design the fluidic network communicating with the channels, for fluidic delivery and experiments.
The project comprise the design of the channel, their fabbrication using a two photon based additive manufacturing and the characterization using the scanning electron microscope and laser vibrometer.
Previous research on this topic was conducted by Lénaic Frehner [1], the report and the achieved results are used as a starting point for this work.

1.2 Suspended microchannel resonators(SMR)

Suspended microchannel resonators are hollow MEMS devices that can be used as mass sensors, they combine a microfluidic channel with a catilever type structure. The working principle is based on the change in the resonant frequency of the resonator when the sample is passing through the channel. The most popular designs are fixed-free beams with microchannels inside (SMR cantilevers) and hollow fixed-fixed beams (bridges) [2].
Lately they drawn growing attention in life science applications like biomedical analysis and biochemical detection [3]. They allow real time measurement in liquid environment with high mass responsivity ideal for detecting bacteria, cells populations, or micron sized analytes.
The fabrication process usually involves the lithography techniques also used for the fabrication of semiconductor devices and can be complex, long and quite costly [4]. Realization of SMR through 3D printing techniques grants a reduction in fabrication time and a cost-effective approach, requiring only one process step. Using polymers also allow easier integration of the biorecognition elements both by incorporation and chemical reaction exploiting the functional groups already present [5]

1.3 3D printing using two photon absorption

1.3.1 Two photon polymerization

This first theoretical part introduce the physical phenomena at the core of the Nanoscribe Photonic Professional GT, the printer used for the fabbrication, and it is mostly based on the slide and my notes relating to this topic of the course: "Advanced additive manufacturing technologies" teached by Professor Christophe Moser.
Two photons polymerization is based on the principle of two photons absorption(TPA), where two photons are absorbed simultaneously, exciting a molecule to a higher energy

state, with the energy gap equal to the sum of the energy of the two incident photons. As showed in Figure 1, the atom goes through an intermediate state called the virtual state for a very small amount of time. To have simultaneous absorption of two photons we need them to be "packed" in time and space. The former condition is obtained using pulsed femtosecond laser, the latter is dependent on the focus of the laser beam.

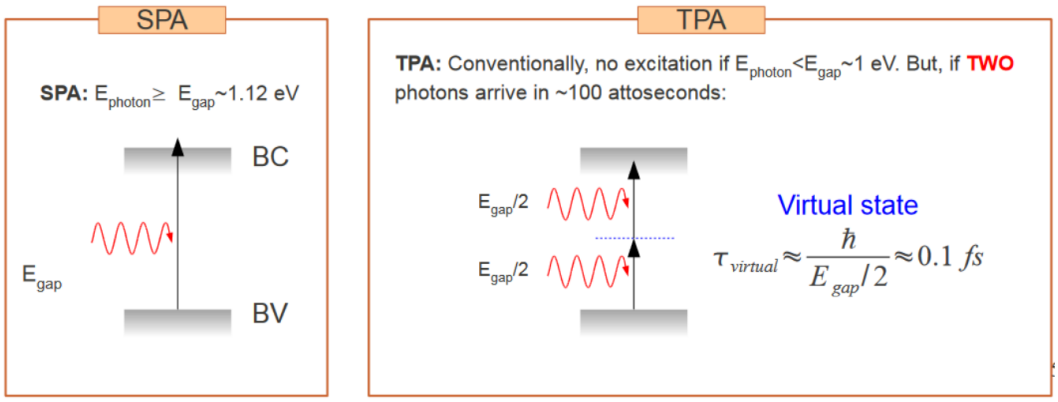

Figure 1: Single and two photons absorption

Compared to Single photon absorbtion(SPA), TPA is a non linear optical process. The number of molecules in excited state is proportional to the square of the laser intensity, and it follows the general formula:

$$\frac{\partial N}{\partial t} = \frac{1}{2}\delta\, N_{GS}\, \frac{I^2}{(h\nu)^2}$$

Where N is the number of excited molecules, δ is the two-photon absorption cross-section, N_{GS} the number of molecules in the ground state and I the laser intensity.
The absorption cross-section is a very small number measured in Goeppert-Mayer(GM) units, $1GM = 10^{-50}\ cm^4\ s\ photon^{-1}$. As a result I need to be big to cause polymerization, meaning that the crosslinking will take place only where the intensity is highest. The excitation by two photons is then confined to a very small volume close to focus, giving rise to a pinpoint 3D resolution far superior to the one in single photon absorption. The difference can be observed in Figure 2 that shows the different fluorescence of the two absorption types.

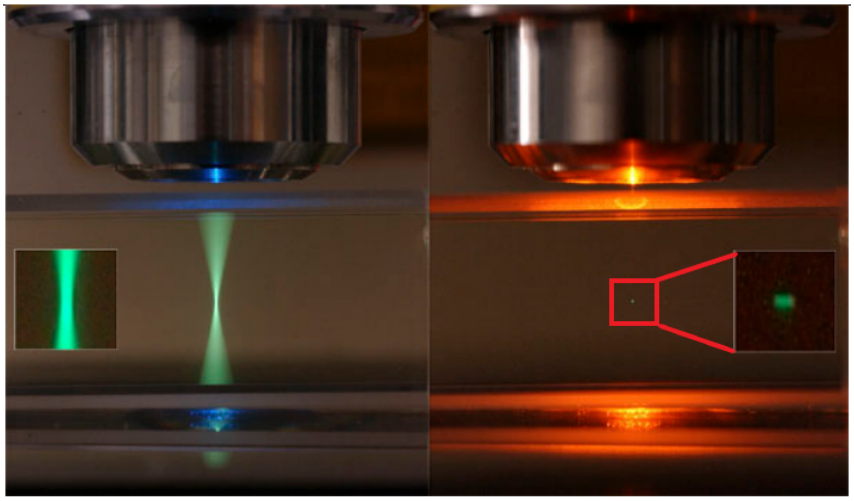

Figure 2: One- vs. two-photon fluorescence.

The photons absorption initiates the polymerization of the photoresin, the minimum polymerized volume is called voxel and it has the shape of a grain of rice. Voxel size is dependent on the dose of the laser, the combination of power and exposure time. Voxels dimensions for a high resolution configuration are typically 700 nanometers for the height and 200 nanometers of maximal diameter.

1.3.2 Equipment description and important parameters

This part describes the main components of the printer and is based on the documentation of the Nanoscribe Photonic Professonal GT provided by the CMi at EPFL.
The setup is composed of a femtosecond laser, a microscope objective and a moving stage, as showed in Figure 3. The laser is fastly scanned on the surface of the substrate trough galvanometric mirrors and it is focused by the objective, building the object layer by layer.The objective is immersed in the resist to avoid refraction effect.Several objectives are available providing different magnifications(10X, 25X, 63X).
Because the scanning surface is small, the substrate can be moved by the piezo-stage, with a travel range of 300µm in all directions during printing. For bigger prints a third displacement mode is available: a coarse stage with a precision around 1.5µm to move between different exposure fields.

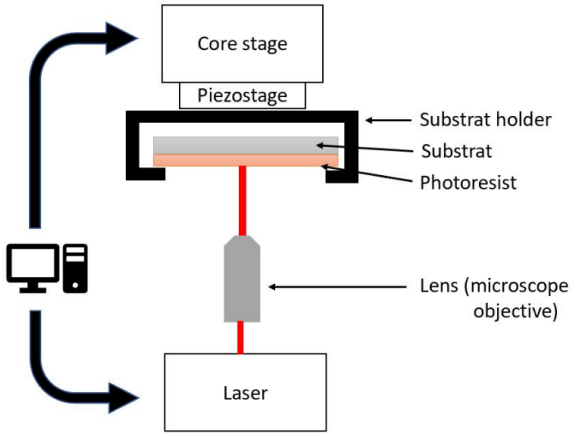

Figure 3: Main components of the printer

The quality of the printed object and the printing time are dependent on some parameters that can be tuned to optimize the result:

- *Laser power*: expressed as a percentage of the total power (150 mW).
- *Scanning speed*: is the velocity at which the surface is scanned by the laser beam.
- *Stage velocity*: the speed of the piezo-stage.
- *Slicing distance*: is the layer height, the distance between each plane, it influences the printing time and the resolution in the z direction.
- *Hatching distance*: is the separation between two consecutive laser beams in the horizzontal plane, it is measured as the distance from the center of one beam to the center of the next beam.
- *Solid/shell and scaffold mode*: the solid mode completely fill the object inside, another possibility is to print only the external shell and the internal supporting structure to avoid the collapse. Shell and scaffold mode is faster but requires additional post processing.
- *Blocks*: If the the printed surface is more than 200μm in X or Y(for the 63x objective), the object must be divided in blocks. Every block is printed from start to finish, then the stage moves to the next one.

1.3.3 Printing workflow

The workflow follows the typical steps of a 3D printed design. There is a first part of computer design(CAD), that in this project was performed with Blender. The resulting STL file is then processed by the software Describe, proprietary of Nanoscribe.
Describe is a slicing software that allows to set all the parameters previously mentioned and to visualize a simulation of the printing process, estimating also the printing time.
The printing start with the preparation of the silicon substrate,that after being polished, undergoes a HDMS treatment to enhance the adhesion of the printed structure. A drop of resist is put on the substrate surface and the sample is loaded in the Nanoscribe. A detailed guide of the preparation steps is available at the CMi website [6].
Once the printing job is over, post processing is required to clean the structure from non-polymerized photoresist, consisting in a bath of Propylene glycol monomethyl ether acetate (PGMEA), followed by a bath in isopropanol alcohol (IPA). A UV post curing could also be necessary to ensure the completely solidification of the object. The post curing can be thermal or UV based, we used a Beltron UV LED chamber [7], available in zone 13 of CMi, to perform the latter, for a duration of 5 minutes.

2 Experimental Procedure

2.1 Printing of single clamped beams

2.1.1 Purpose

The purpose of this experiment is finding the optimal parameters for printing suspended single clamped beams, using as starting point Leniac's results and design.

2.1.2 Design and Methodology

An array of eighteen beams with different characteristics was design in order to evaluate the effect of the geometry on the printing outcome as represented in Figure 4.
The chosen tested geometries are:

- Length of the channel: 50 μm and 100 μm
- Cross section: 5 μm, 10 μm and 20 μm
- Wall thickness: 2 μm, 1 μm and 500 nm

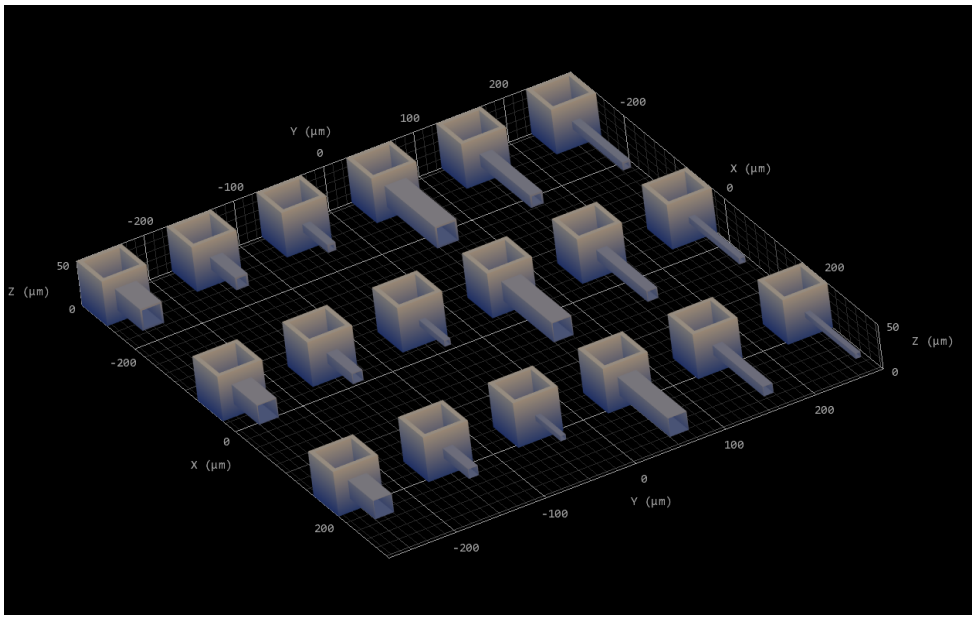

Figure 4: Describe view of the array of resonators

Name	Value	Name	Value
SlicingDistance	0.3 μm	StageVelocity	10 μm/s
HatchingDistance	0.2 μm	HatchingAngle	0°
LaserPower	40%	ScanSpeed	10000 μm/s

Table 1: Important parameters for the first print

Table 1 shows a summary of the major parameters for the printing procedure. The slicing distance, laser power and scan speed are set following the recommended values for the 63X objective. The stage velocity is set to 10 μm/s instead of the recommended value 200 μm/s, because the latter causes a bending of the suspended structures as found by Leniac [1]. The hatching angle is defined as the angle between the y-axis and the laser scanning direction,it is critical in suspended parts and, in this particular design, needs to be set at 0 degrees to avoid the printing of single long suspended lines (the same is not necessarily true also for double clamped beams). As shown in Figure 5 and 6, an hatching angle equals to 90 degrees will affect the laser scanning direction, the first polymerized line will have a length equal to the channel length and just a single point of contact with the base structure. On the contrary on Figure 6, we can observe that the consecutive lines are shorter and the first line has a better contact with the blue object. However even this method does not prevent bending if the channel is too long.

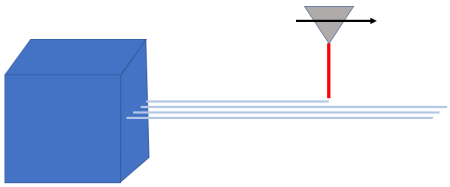

Figure 5: Hatching angle = 90°

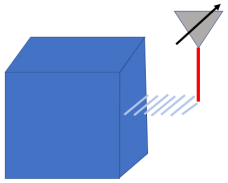

Figure 6: Hatching angle = 0°

Not being sure about the critical length before bending, we decided to divide the 100μm channels in two different blocks. In this way the second half of the channel is printed after some time from the first part, that will be mechanical more stable.The solid mode was chosen because the estimated time reduction using the shell and scaffold mode was not substantial.

The printing was performed on the Nanoscribe with the 63X objective and the IP-dip photoresist, the printing time was around one hour and fifteen minutes.

2.1.3 Result of the first attempt

In Figure 7, taken with the optical microscope, we can see the whole array. On the top half there are the 50 μm long channels and on the bottom the 100 μm long ones. The thickness is increasing with the numbers, column 1 is the 500 nm, 2 is 1μm and 3 is 2μm. Major defects are visible, even with this low magnification, through the entire column 1. The 50 μm channels of column 2 and 3 shows no major defects, just a stitching effect due to the division of the single channel in two blocks. The longer channels of 2μm are properly printed, while some of the channels of 1μm are bend to the ground, as shown by the red rectangle on Figure 8

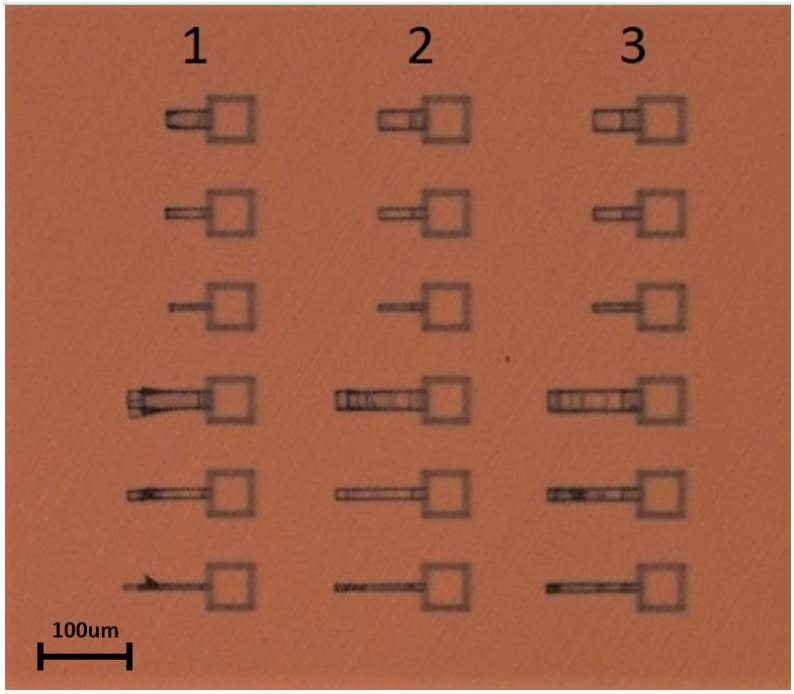

Figure 7: Overview of the first print. 1: 500nm thickness. 2: 1μm thickness. 3: 2μm thickness

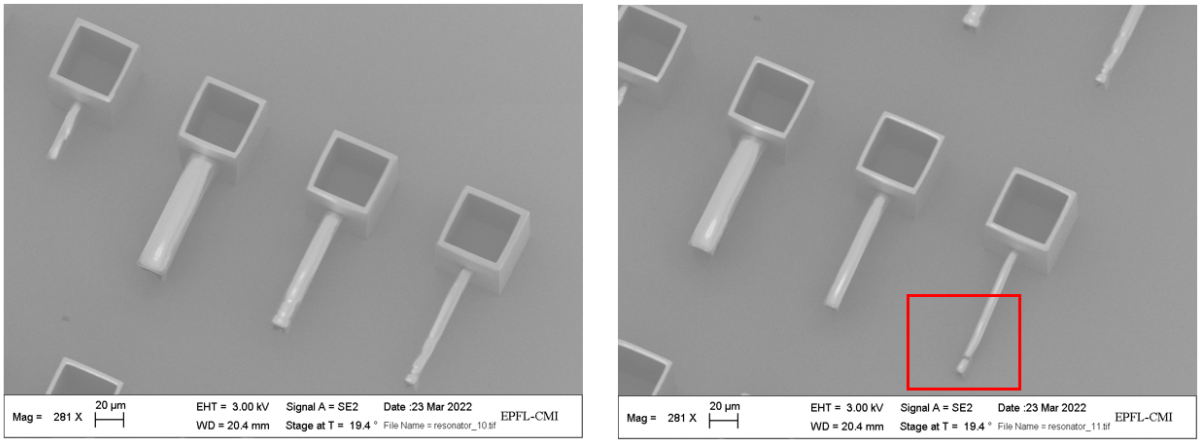

Figure 8: Left, 2μm thickness. Right 1μm thickness

To avoid these defects in the next printing, every beam was printed in a single block, the Slicing Distance was set in adaptive mode with a value between 0.3 and 0.1 μm as done by Leniac [1]. It was also decided to not reprint the 2μm wall thickness because the quality was already satisfactory, focusing instead on sub-micrometer walls.

2.1.4 Result second printing

As can be seen in Figure 9, the new parameters resulted in an overall worse quality. For example, comparing the two columns of the 500nm thickness channels in this Figure and Figure 7, there are more noticeable defects, corresponding to the blacked areas.

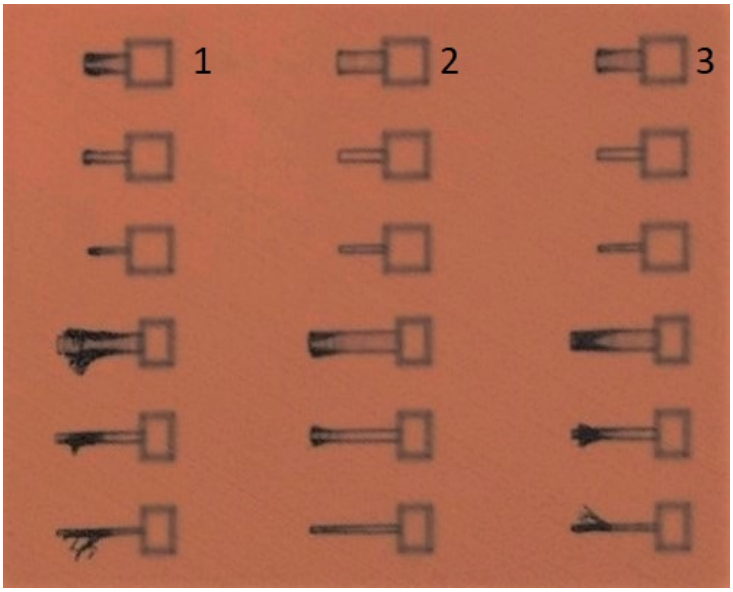

Figure 9: Overview of the second printing. 1: 500nm thickness. 2: 1μm thickness. 3: 750nm thickness

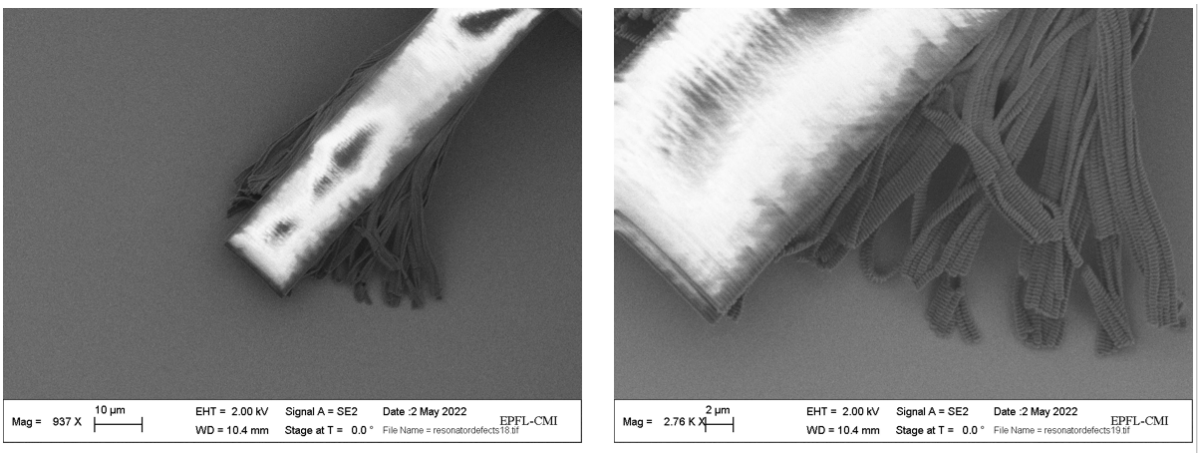

Figure 10: Details of a 500 nm collapsed channel

Figure 10 is a SEM close view of one of the collapsed channel, the white area is an effect of charging because the photoresist is not conductive. In the right part of the image we are able to see the single voxels composing the printed misplaced lines.

2.1.5 Final parameters and Discussion

Name	Value	Name	Value
SlicingDistance	0.2 μm	StageVelocity	10 μm/s
HatchingDistance	0.2 μm	Mode	Shell and Scaffold
LaserPower	40%	ScanSpeed	10000 μm/s

Table 2: Optimal printing parameters

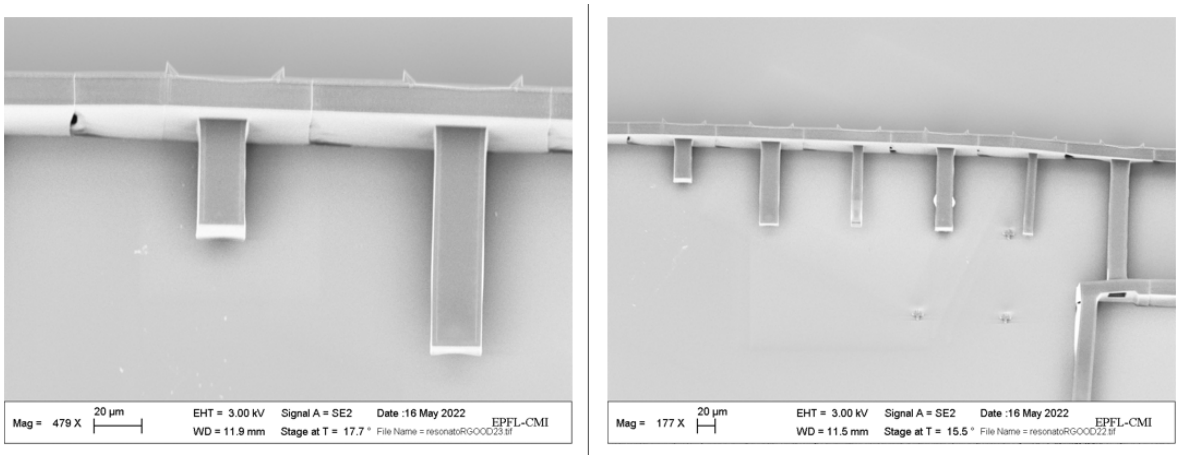

Figure 11: Left, 500nm(left) and 1μm thick walls. Right, overview

The shell and scaffold mode and the lower slicing distance were the two major changes in the parameters (Table 4). With this new parameters the printing was good even for 500 nm thickness (Figure 11). Every resonator was delimited by a single block.
With the lower slicing distance, the bottom side of the channel is composed of more layers ensuring a reduced tendency to bend, eventually resulting in better quality.
It can be concluded that the adaptive slicing mode, that should have increased the quality in the second print, is only suitable for curved structures, and it has no effect on 90 degrees angles.
Finally shell and scaffold mode seems to be an important parameter, not just for decreasing the printing time, but also for the suspended structures, this could be a aftermath of the peculiar scanning trajectory of the laser in this mode, that combine hatching angles of 0 and 90 degrees.

2.2 Printing of clamped-clamped beams

The parameters selected in the previous paragraph were used for the fabrication of double clamped beams (bridges) of 100μm and 150μm length and different walls thickness(1μm, 750nm, 500nm), with optimal results, as shown in Figure 12 and Figure 13.
In general, printing of bridges was easier than cantilever, providing better quality and higher repeatability. This is mostly due to the fact that bridges have a lower tendency to bend and are less fragile than single clamped beams, thanks to the two anchor points.

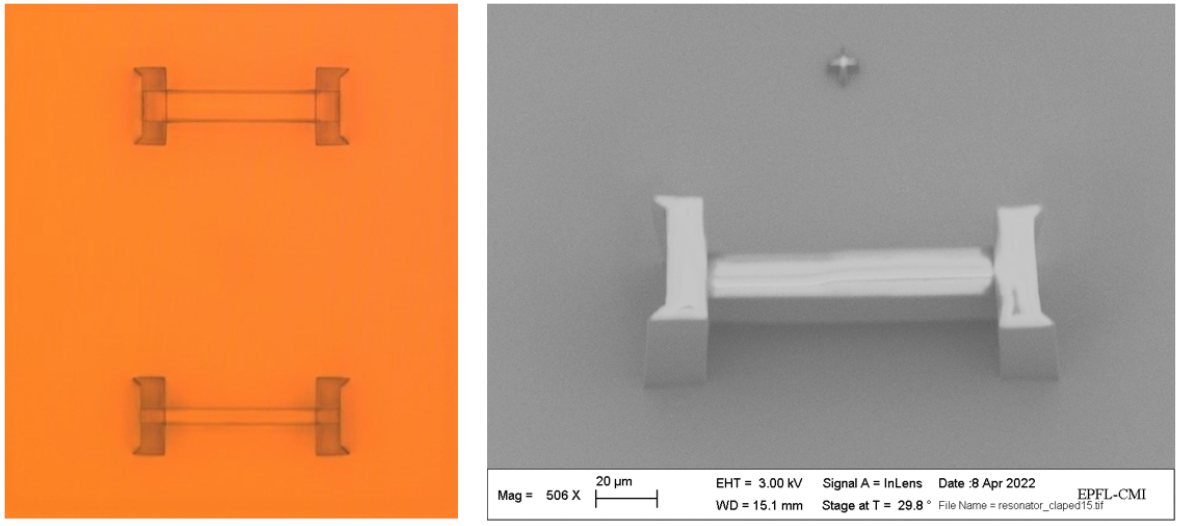

Figure 12: Left, two bridges of 500nm thickness. Right, SEM image of a bridge

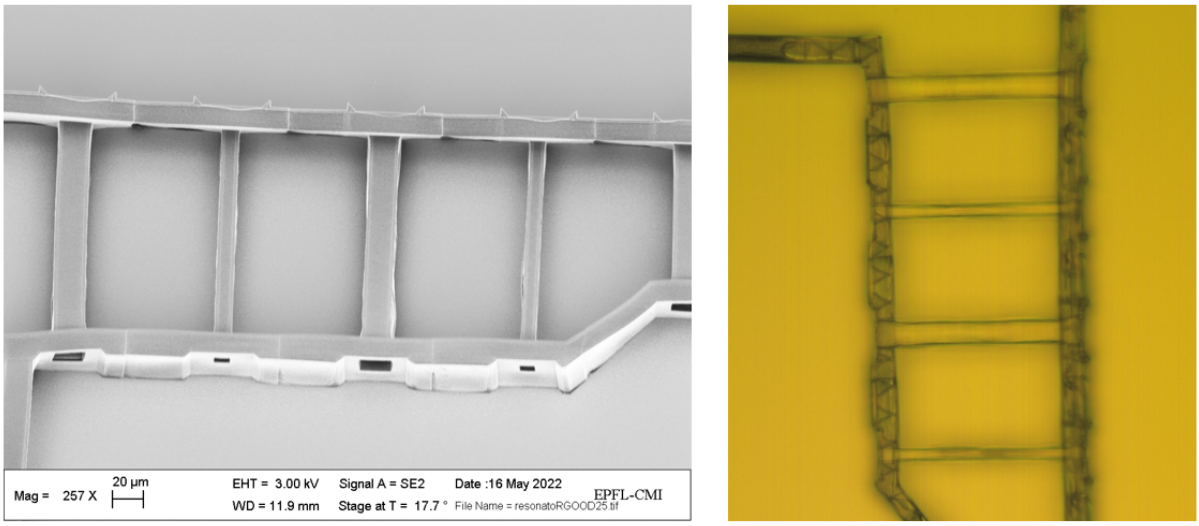

Figure 13: 150 μm long double clamped beams

2.3 Integration of a fluidic delivery system

Once the resonator are correctly printed, we need to design and implement a system to deliver a liquid sample inside the channel. We thought of connecting the suspended channels to a bigger cubic reservoir of approximately $1mm^3$ of volume. The big dimension of the reservoir can allow measurements before the complete evaporation of the liquid sample.

2.3.1 Alignment experiment

The resonators and the reservoir cannot be printed at the same time. The 63X objective allows printing of structures of maximal volume around $0.1mm^3$ [6], because of the high

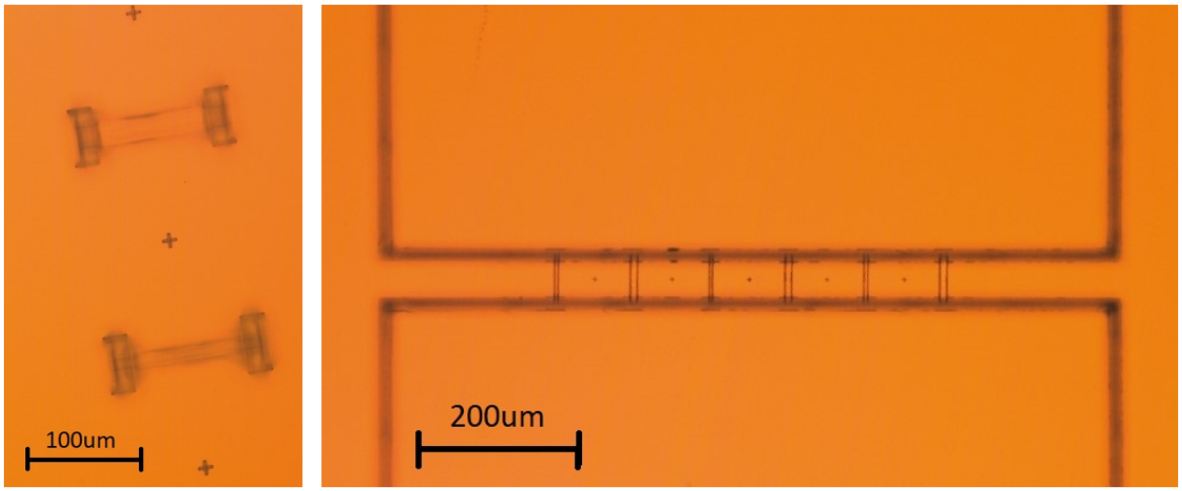

Figure 14: Left, the crosses for the alignment. Right, top view of the reservoirs.

resolution of this objective it would take ages to print a millimetric size structure. The solution is printing first the resonator with the high resolution objective and than print on top the reservoir, using the less precise but faster 25X objective with the IP-S resist. To correctly position the reservoir on top of the SMRs we followed the alignment manual of the Nanoscribe (method 2), in particular we printed some crosses to use as a reference coordinates.

The alignment was successful as can be seen in Figure 14, but the walls of the two cubic structures were only 200 μm tall, instead of 1 mm. At first we thought that the cause was to be found in the thickness of the walls of 30μm, that could had caused a collapse of the structure. But repeating the print with thicker walls we encountered the same problem. Eventually, changing the z-axis movement of the stage from "Piezo" to "Microscope drive" in the software, we were able to obtain a satisfactory result.

Name	Value	Name	Value
Wall thickness	70 μm	Z-drive	Microscope
Block size x-y	200 μm	Edge	1mm
Block size z	250 μm	Mode	Shell and scaffold

Table 3: Parameters for the reservoir printing

2.3.2 Channel development

As already mentioned, the resonators go trough a development step in PGMEA after the end of the printing process. In order to prove the full development of the inside of the hollow beams, we put a small drop of IPA on our samples to observe the fill. All the resonators correctly filled in the presence of liquid. In particular in Figure 15 we can observe the air bubbles coming out of the first and the last resonator as a result of the filling process. It can be said , than, that the development time of 17 minuted is sufficient for beams of 5μm or more of cross section.

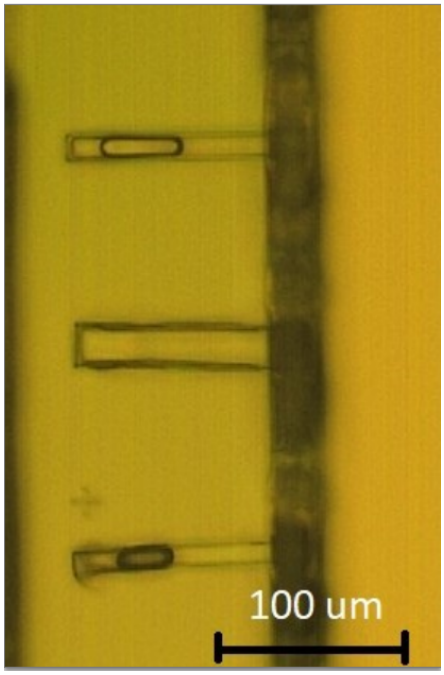

Figure 15: Detail of the resonators filling

2.3.3 Confinement of the liquid

The water tightness of the reservoir is dependent on the printing parameters and the design of choice. To determine it, a small amount of liquid was dropped outside the reservoir and the behaviour of the water front was observed. As can be seen from Figure 16, The IPA can pass through the printed walls and under them. If the liquid cannot be constrained inside the reservoir the measurement of the resonance frequency of the beams becomes impossible because they are completely submerged.

By adding a floor layer of a few micrometers thickness to the design the infiltration from below could be solved. The leakage through the walls can be explained looking back at Figure 11. The printed structure presents some defects corresponding to the boundary between different blocks, these holes in the shell jeopardize the water tightness. Because the shell and scaffold mode was used, the walls are mostly empty inside, and a hole in the shell is detrimental for the structure, choosing the solid mode can be the solution, but it results in a doubling of the printing time, that is already over two hours. An other possibility could be to increase the shell thickness just enough to avoid the effect of possible defects, without sacrificing speed.

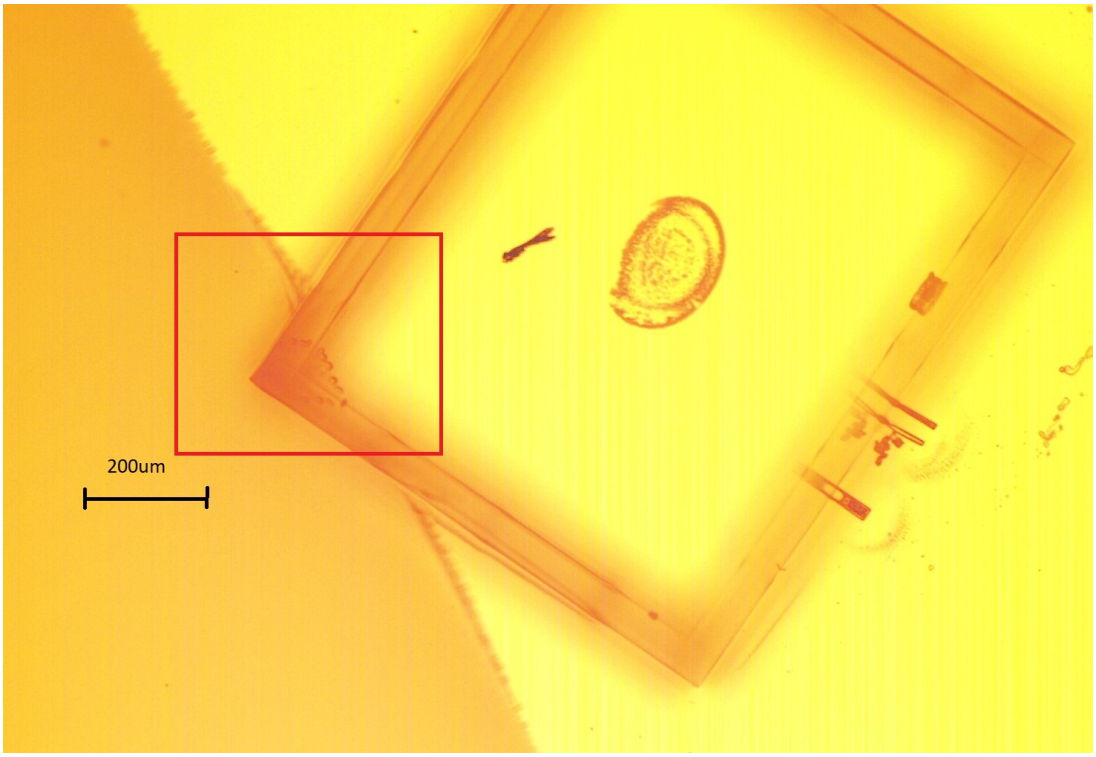

Figure 16: IPA infiltrating in the reservoir

3 Simulations and Measurements

Once good printing quality is achieved, we can measure the resonant frequency of the SMRs through Laser Doppler Vibrometry(LDV), that allows a thermo-mechanical(TM) noise analysis. TM noise represents stochastic oscillations of the cantilever caused by Brownian motion of the cantilever itself and other dissipative mechanisms for a given temperature. [8] Laser doppler vibrometry is based on interferometry, that uses optical interference to measure the frequency or phase difference of the test signal and the reflected one by the moving object, it allows femtometer amplitude resolution and is linear, having a consistent amplitude also for the high frequency ranges.
Because the problems with the reservoir could not be solved in time, the measurements were performed without a liquid sample inside the beams.

3.1 Transparency problem

On the first measurement attempt, we could not get any data. The problem resides in the transparency of the cured photoresist to the laser beam, that passes though the structure and gives back the TM noise of the underlying silicon substrate.

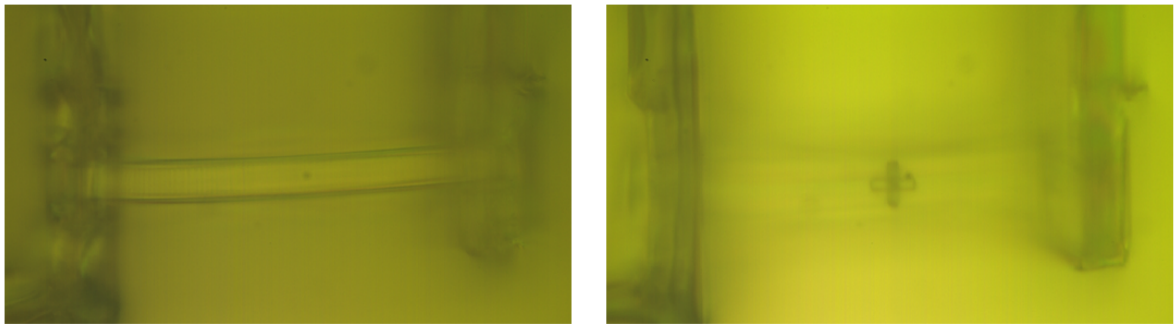

Figure 17: Left,focus on the beam. Right, focus on the substrate

As can be seen in Figure 17, taken with a optical microscope, changing the focus of the microscope we are able to see through the resonator, and focus on the thin cross that is at the surface of the silicon chip.
In order to solve this problem we decided to sputter 10 nm of aluminum on the surface of the chip, using the Pfeiffer SPIDER 600, that allows deposition of thin layers of metallic material on silicon chips [9]. The chip was secured to a 100 mm wafer(the only dimension compatible with the machine) with some Kapton tape, and it was subject to an aluminum sputtering process at room temperature, with a power of 1000W for 6 seconds.

3.2 Single clamped beams

After adding the aluminum thin film we were able to determine the resonant frequency of the single clamped beams. We also simulated a simple model of the cantilever with COMSOL multiphysics(Figure 18), to have some reference values. The simulation is not taking into account the effect of air damping on the resonant frequency, we then expect to obtain lower values than the simulated ones.
In order to simulate the model we need to define the key mechanical properties of the photocured resist IP-Dip:

- Young's modulus: 4.5 GPa
- Poisson 's ratio: 0.35
- Density: 1.2 g/cm^3

Taken from the article: "Deformation Behavior of Foam Laser Targets Fabricated by Two-Photon Polymerization" [10] by Ying Liu. We also included a fixed constraint on one side to simulate the anchor point of the resonator.

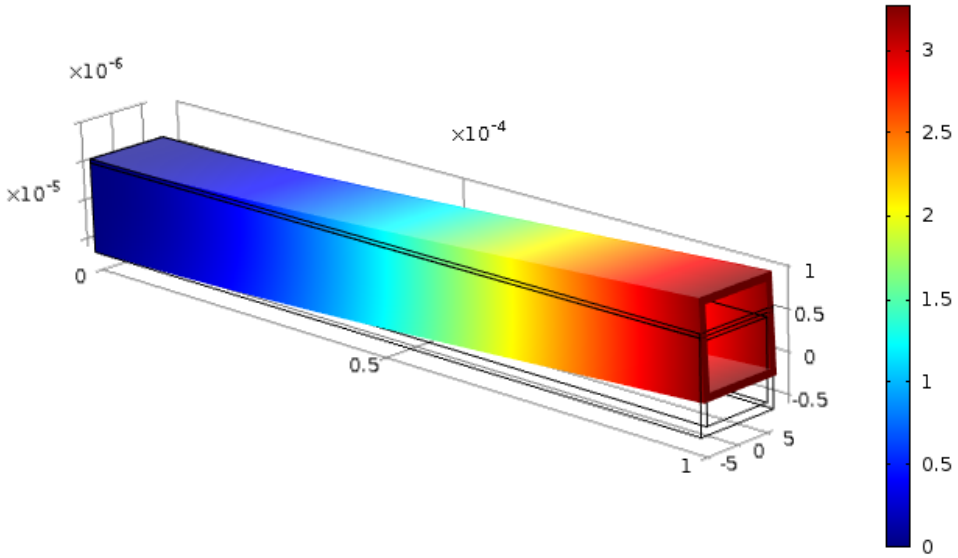

Figure 18: COMSOL model used for the simulation

Length	Cross section(μm)	Thickness(μm)	Identifier
50	5	0.5	R1
50	20	0.5	R2
100	10	2	R3
100	10	1	R4
100	10	0.5	R5
100	5	1	R6
100	20	0.5	R7

Table 4: Different type of measured resonators

3.3 Results

Table 4 and Table 5 summarize the different types of resonator measured and the outcome of the LDV measurments. As expected the Simulated frequency has a higher value than the measured one, nonetheless we can observe that both values follow the same trends for different geometries.

Identifier	Measured Res. freq	Simulated Res. freq.
R1	818 kHz	950 kHz
R2	980 kHz	1.14 MHz
R3	369 kHz	475 kHz
R4	333 kHz	470 kHz
R5	313 kHz	452 kHz
R6	176 kHz	260 kHz
R7	596 kHz	787 kHz

Table 5: Results of the resonant frequency measurement

From theory we know that the resonant frequency of a simple rectangular cantilever beam is expressed as:

$$f_0 = \frac{1}{2\pi}\sqrt{\frac{EI}{\rho AL^4}} \tag{1}$$

Where E is the Young modulus, I is the inertia, ρ is the density, A is the area of the cross section and L in the length of the cantilever.I can also be written as [1]:

$$I = \frac{a_{out}^4 - a_{in}^4}{12} \tag{2}$$

Where a_i is the edge of the square.
We then expect a lower resonance frequency as the length of the cantilever grows, as verified by R2 $>$ R7. Following Equation 1, we would expect the resonance frequency to go down by a factor of 4, indeed the geometry is more complex, so we can use the results of the simulation to analyze the correctness of the measures. In particular we can observe that both values go down by approximately a factor of 1.5.
In accordance with theory, when the thickness of the walls increases (larger a_{out} same a_{in}) the resonance frequency increases because of the larger value of I, as verified by R5 $<$ R4 $<$ R3. Lastly we expect to find higher resonance frequency for higher cross section with the same walls thickness, as confirmed by R2 $>$ R1, R5 $>$ R7 and R4 $>$ R6.
It can therefore be said that the LDV can be used to correctly measure the resonance frequency of cantilever beams, however is not suitable for bridges because of their low movement under the influence of TM noise. The obtained values are in accordance with

theory and the discrepancy between measured and simulated one can be considered as an offset resulting from the oversimplified COMSOL model.

3.4 Double clamped beams

Despite adding the metallic layer we were not able to measure the bridges resonant frequency. This could depends on the fact that these structures are doubled constrained so they move less under the effect of TM noise. We simulated the resonance frequency with COMSOL with the same parameters as before,and adding a second constraint on the side of the beam, the result are summarized in Table 6.

Length	Cross section(μm)	Thickness(μm)	Simulated Res. Freq.
100	5	0.5	1.45 MHz
100	10	0.5	2.32 MHz
100	5	1	1.59 MHz
100	10	1	2.45 MHz
150	5	0.5	670 kHz
150	10	0.5	1.17 MHz

Table 6: Results of the simulation of different type of bridges

As before the model is not taking into account the effect of air damping so the real values are probably lower.

4 Conclusion

Testing different parameters, we were able to have new insights on the fabrication of suspended microchannel resonators with a 2 photon 3D printer. We successfully printed resonators of 500 nm walls thickness, single and double clamped.
We investigated the possibility to implement a fluidic delivery system to the resonators, understanding the most important parameters and techniques to take into consideration when printing a millimetric size reservoir to ensure water tightness and reasonable printing speed.
Concerning the measurements, we were able to measure the resonance frequency of single clamped beams, with laser doppler vibrometry, by adding a thin layer of aluminum that makes the structures reflective. The measurements of double clamped beams , on the other hand, were unsuccessful, possible causes and solution need to be further investigated. The values obtained with the measurements are in accordance with the theory and the simulated models.

References

[1] Optimization of channel design and fabrication for suspended microchannels resonators with a 3d nanoprinter. https://infoscience.epfl.ch/record/267987. Accessed: 2022-04-24.

[2] Celso Accoto, Antonio Qualtieri, Ferruccio Pisanello, Carlo Ricciardi, Candido Fabrizio Pirri, Massimo De Vittorio, and Francesco Rizzi. Two-Photon Polymerization Lithography and Laser Doppler Vibrometry of a SU-8-Based Suspended Microchannel Resonator. *Journal of Microelectromechanical Systems*, 24(4), 2015.

[3] Davide Scaiola, Stefano Stassi, Roberta Calmo, Damien Maillard, Stefano S.G. Varricchio, Annalisa De Pastina, Guillermo Villanueva, Philippe Renaud, and Carlo Ricciardi. Fabrication of clamped-clamped beam resonators with embedded fluidic nanochannel. *Microelectronic Engineering*, 231, 2020.

[4] Annalisa De Pastina and Luis Guillermo Villanueva. Suspended micro/nano channel resonators: A review, 2020.

[5] Stefano Stassi, Erika Fantino, Roberta Calmo, Annalisa Chiappone, Matteo Gillono, Davide Scaiola, Candido Fabrizio Pirri, Carlo Ricciardi, Alessandro Chiadò, and Ignazio Roppolo. Polymeric 3D Printed Functional Microcantilevers for Biosensing Applications. *ACS Applied Materials and Interfaces*, 9(22), 2017.

[6] Nanoscribe photonic professional gt+. https://www.epfl.ch/research/facilities/cmi/equipment/pho photonic-professional-gt/. Accessed: 2022-05-22.

[7] Beltron uv led chamber. https://www.epfl.ch/research/facilities/cmi/wp-content/uploads/2021/09/Beltron.manual.pdf. Accessed: 2022-06-04.

[8] Zoran G. Djurić and Ivana M. Jokić. Thermomechanical noise of nanooscillators with time-dependent mass. *Microelectronic Engineering*, 84(5-8), 2007.

[9] Pfeiffer spider 600. https://www.epfl.ch/research/facilities/cmi/equipment/thin-films/pfeiffer-spider-600/. Accessed: 2022-05-20.

[10] Ying Liu, John H. Campbell, Ori Stein, Lijia Jiang, Jared Hund, and Yongfeng Lu. Deformation behavior of foam laser targets fabricated by two-photon polymerization. *Nanomaterials*, 8(7), 2018.